ELSEVIER

Rotor-synchronized acquisition of quadrupolar satellite-transition NMR spectra: practical aspects and double-quantum filtration

Sharon E. Ashbrook [a], Stephen Wimperis [b,*]

[a] *Department of Earth Sciences, University of Cambridge, Downing Street, Cambridge CB2 3EQ, UK*
[b] *Department of Chemistry, University of Exeter, Stocker Road, Exeter EX4 4QD, UK*

Abstract

The very broad resonances of quadrupolar (spin $I > 1/2$) nuclei are resolved by magic angle spinning (MAS) into a large number of spinning sidebands, each of which often remains anisotropically broadened. The quadrupolar interaction can be removed to a first-order approximation if the MAS NMR spectrum is acquired in a rotor-synchronized fashion, aliasing the spinning sidebands onto a centreband and thereby increasing the signal-to-noise ratio in the resulting, possibly second-order broadened, spectrum. We discuss the practical aspects of this rotor-synchronization in the direct (t_2) time domain, demonstrating that the audiofrequency filters in the receiver section of the spectrometer have a significant impact on the precise timings needed in the experiment. We also introduce a novel double-quantum filtered rotor-synchronized experiment for half-integer spin quadrupolar (spin $I = 3/2$, 5/2, etc.) nuclei that makes use of central-transition-selective inversion pulses to both excite and reconvert double-quantum coherences and yields a simplified spectrum containing only the ST_1 ($m_I = \pm 1/2 \leftrightarrow \pm 3/2$) satellite-transition lineshapes. For spin $I = 5/2$ nuclei, such as ^{17}O and ^{27}Al, this spectrum may exhibit a significant resolution increase over the conventional central-transition spectrum.
© 2005 Elsevier Inc. All rights reserved.

Keywords: Quadrupolar NMR; Satellite transitions; Rotor synchronization; Double-quantum filtration; Magic angle spinning

1. Introduction

NMR spectra of powdered solids are often dominated by very large anisotropic broadenings arising from dipolar, chemical shift and, for spin $I > 1/2$ nuclei, quadrupolar interactions [1]. The most widely adopted approach to improving resolution in solids is to suppress the first-order effects of these interactions using magic angle spinning (MAS), i.e., rapid rotation of the powder about an axis inclined at an angle $\chi = 54.736°$ to the external magnetic field [1,2]. To remove first-order broadenings completely, the MAS rate must be much greater than the magnitudes of the relevant anisotropic interactions [2,3]. Spinning rates of up to 35 kHz are currently achievable on typical commercial probes and are sufficient to suppress many dipolar and chemical shift interactions. For spin $I > 1/2$ nuclei, however, the quadrupolar interaction is usually dominant and may produce anisotropic broadenings up to several MHz [4]. In cases, where the MAS rate is slower than the magnitude of the interaction, an "inhomogeneously broadened" powder lineshape is split up into a series of spinning sidebands, equally spaced at the spinning frequency [1,3].

For spin $I > 1/2$ nuclei with half-integer spin quantum number I, the quadrupolar interaction results in two distinct types of single-quantum transition [4]. The frequency of the central transition (or CT), $m_I = +1/2 \leftrightarrow -1/2$, is not perturbed by the quadrupolar interaction to a first-order approximation. However, the frequencies of the satellite transitions, ST_1 with $m_I = \pm 1/2 \leftrightarrow \pm 3/2$, ST_2 with $m_I = \pm 3/2 \leftrightarrow \pm 5/2$, ..., etc., show a strong dependence upon the quadrupolar

---

* Corresponding author. Fax: +44 1392 263434.
E-mail address: s.wimperis@exeter.ac.uk (S. Wimperis).

interaction. In a frame rotating at the Larmor frequency, v_0 the frequency of a single-quantum transition $m_I = \pm (q-1) \leftrightarrow \pm q$, with $q = 1/2, 3/2, 5/2, \ldots$, etc., is given, to first order, by [5]

$$v_{\pm(q-1)\leftrightarrow\pm q}^{(1)} = \pm(2q-1)v_Q^{PAS}d_{0,0}^2(\theta), \qquad (1)$$

with the quadrupolar splitting parameter

$$v_Q^{PAS} = 3e^2qQ/4I(2I-1)h. \qquad (2)$$

Axial symmetry of the quadrupole tensor ($\eta = 0$) has been assumed for simplicity here. The angle θ describes the orientation of the principal axis system (PAS) of the quadrupole tensor in the laboratory frame. In a powdered solid, this orientational dependence results in a large anisotropic broadening of the satellite transitions. This can be seen in Fig. 1A, a computer-simulated spin $I = 3/2$ powder lineshape. The central transition, with $q = 1/2$, is narrow, whilst the satellite transitions, with $q = 3/2$, are broadened. Fig. 1 also shows the effect of MAS upon this lineshape. The satellite transitions split into a series of sharp spinning sidebands, equally spaced at the spinning frequency (10 kHz in Fig. 1B and 20 kHz in Fig. 1C), with intensities that, at slow MAS rates, re-

A

B

C

Fig. 1. Spin $I = 3/2$ powder-pattern NMR lineshapes, simulated with $C_Q = e^2qQ/h = 0.4$ MHz and $\eta = 0.0$, under (A) static and (B and C) MAS conditions, with MAS rates, v_R, of (B) 10 kHz and (C) 20 kHz. Central and satellite transitions are indicated by CT and ST, respectively.

flect the static lineshape. These spinning sidebands have been used to obtain accurate quadrupolar parameters in systems with moderate quadrupolar couplings [6].

When the magnitude of the quadrupolar interaction is large, the spectrum can no longer be described solely in terms of the first-order approximation and consideration of the second-order contribution to the energy levels is required [4,5]. The frequency of a single-quantum transition becomes the sum of first- and second-order terms [5]

$$v_{\pm(q-1)\leftrightarrow\pm q} = v_{\pm(q-1)\leftrightarrow\pm q}^{(1)} + v_{\pm(q-1)\leftrightarrow\pm q}^{(2)} \qquad (3)$$

with, assuming $\eta = 0$,

$$v_{\pm(q-1)\leftrightarrow\pm q}^{(2)}$$
$$= \frac{(v_Q^{PAS})^2}{v_0}\left\{A^0(I,q) + A^2(I,q)d_{0,0}^2(\theta) + A^4(I,q)d_{0,0}^4(\theta)\right\}. \qquad (4)$$

The spin-dependent coefficients $A^l(I,q)$ can be found in the literature [5]. The second-order quadrupolar correction to the transition frequency, $v_{\pm(q-1)\leftrightarrow\pm q}^{(2)}$, which affects all transitions, can be seen to consist of both an isotropic shift (proportional to $A^0(I,q)$) and an anisotropic broadening (with both rank $l = 2$ and $l = 4$ terms). The second-order quadrupolar interaction is much smaller than the first-order interaction as it is proportional not to v_Q^{PAS}, but to $(v_Q^{PAS})^2/v_0$, where usually $v_Q^{PAS} \ll v_0$.

Owing to its more complex angular dependence, second-order quadrupolar broadening cannot be removed completely by MAS alone [4,5]. If MAS is assumed to be infinitely fast, both anisotropic first-order and $l = 2$ second-order broadening are removed, but the $l = 0$ isotropic shift and the $l = 4$ broadening remain. The MAS-averaged single-quantum transition frequency then becomes [5]

$$\langle v_{\pm(q-1)\leftrightarrow\pm q}\rangle_{MAS}$$
$$= \frac{(v_Q^{PAS})^2}{v_0}\left\{A^0(I,q) + A^4(I,q)d_{0,0}^4(\beta)d_{0,0}^4(\chi = 54.736°)\right\}, \qquad (5)$$

where β describes the orientation of the quadrupolar PAS in a rotor-fixed frame. This results in an anisotropically broadened lineshape such as that shown in Fig. 2A, a spin $I = 5/2$ central-transition powder lineshape. In principle, at infinitely high spinning rates, similar lineshapes will also be obtained for the spin $I = 5/2$ satellite transitions, ST_1 ($q = 3/2$) and ST_2 ($q = 5/2$), but with differing isotropic and anisotropic contributions given by the respective coefficients $A^l(I,q)$ [6,7]. In practice, however, the magnitude of the first-order quadrupolar broadening ensures that MAS rates are slow relative to the anisotropic linewidth and the numerous satellite-transition spinning sidebands described
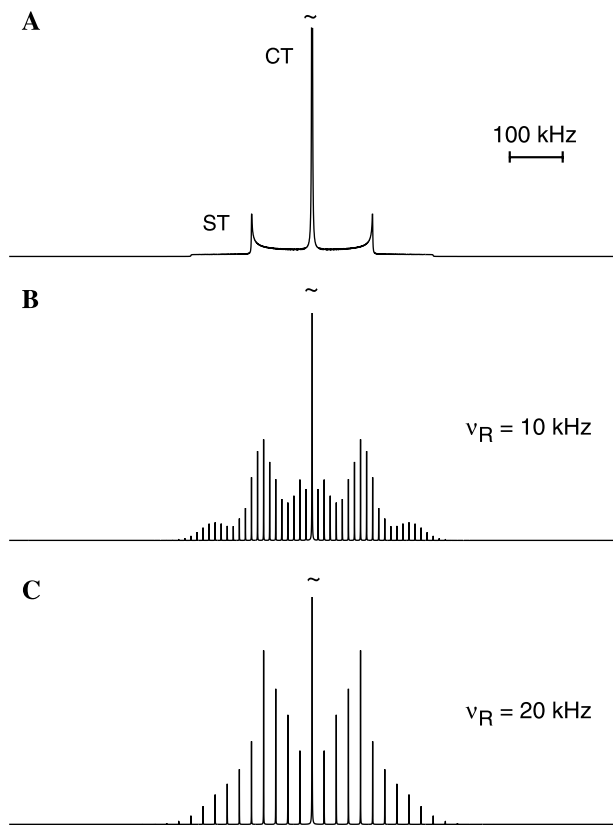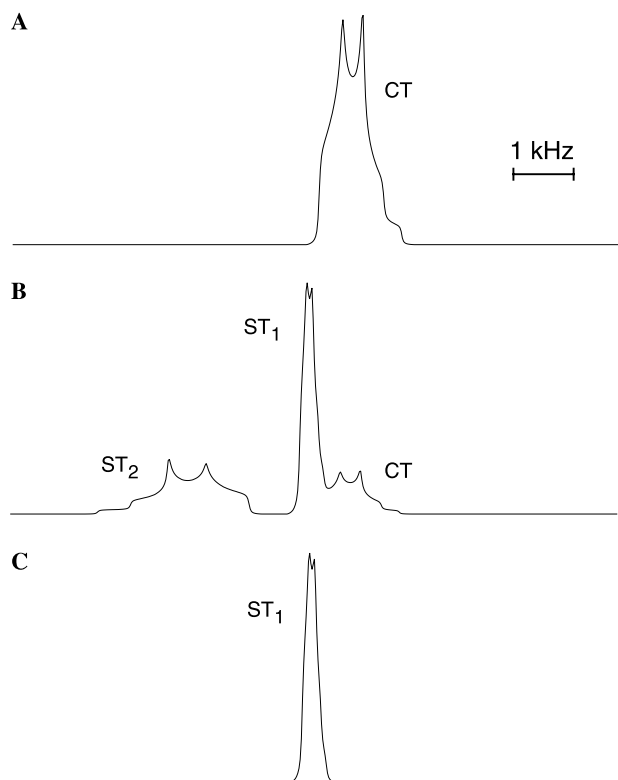
A

B

C

Fig. 2. Spin $I = 5/2$ MAS NMR lineshapes simulated (assuming infinitely fast MAS) with $C_Q = 3.0$ MHz, $\eta = 0.5$ and $\nu_0 = 100$ MHz. Central and satellite transitions are indicated by CT, ST_1 (for $q = 3/2$) and ST_2 (for $q = 5/2$), respectively. In (A), only the central-transition lineshape is present, whilst the spectrum in (B) is that which would result from a rotor-synchronized acquisition, with all three transitions present with significant intensity. In (C), the spectrum contains only the ST_1 satellite-transition lineshape, as would result from a double-quantum filtered rotor-synchronized acquisition.

previously will be obtained, with each sideband exhibiting a second-order powder lineshape [6].

It is possible to remove fully the first-order broadening at slower spinning rates through the use of rotor-synchronization. In the time domain this involves the acquisition of data in concert with the rotor period, thereby sampling only the tops of the rotary echoes. Or alternatively, considered in the frequency domain, the spectral width is chosen to be equal to the spinning frequency, ν_R, resulting in the "folding" or "aliasing" of spinning sidebands onto the centreband as a consequence of the Nyquist theorem [8]. The spectrum which would result from such a synchronized acquisition is shown in Fig. 2B, simulated for a spin $I = 5/2$ nucleus. Three distinct lineshapes are now observed, the central (CT) transition and two satellite transitions (ST_1 and ST_2), each broadened only by the second-order quadrupolar interaction. In addition to exhibiting inherently different intensities, each lineshape also possesses a different isotropic shift and anisotropic broadening, reflecting the differences (in both sign and magnitude) of the $A^0(5/2, q)$ and $A^4(5/2, q)$ coefficients, respectively [5,7].

In particular, the anisotropic broadening associated with the spin $I = 5/2$, $q = 3/2$ satellites (ST_1) is particularly small, with $A^4(5/2, 3/2) = (7/24) A^4(5/2, 1/2)$, resulting in a narrow linewidth compared with the central transition. This can result in increased resolution when more than one crystallographically distinct species is present, even in amorphous/disordered solids where the resonances are often broadened by a distribution of the quadrupolar interaction.

This increase in resolution for the specific case of spin $I = 5/2$ ST_1 satellite transitions has been widely exploited in the literature [7,9,10] and the method has been dubbed "satellite-transition spectroscopy" (SATRAS) [9]. It is possible to look at an individual satellite-transition spinning sideband to resolve, or partially resolve, distinct species which may be overlapped in the conventional central-transition lineshape. However, consideration of only one of the many satellite-transition spinning sidebands results in an inherently low sensitivity, estimated to be an order of magnitude lower than that of the central-transition MAS lineshape [9]. Furthermore, when second-order quadrupolar interactions are present, the lineshape obtained for an individual sideband is not necessarily representative of the true "infinitely fast MAS" powder-pattern lineshape [3,6]. In contrast, when all sidebands are aliased in a rotor-synchronized experiment, sensitivity may be significantly improved and the ideal lineshape obtained.

Although of particular interest for spin $I = 5/2$ ST_1 satellites, the more general study of satellite-transition lineshapes is also of importance. They provide an additional, independent measurement of the isotropic chemical shift and quadrupolar parameters owing to their different isotropic and anisotropic contributions [9]. Furthermore, they are affected by a number of high-order interactions (such as quadrupolar-shielding cross-terms [11]) differently to the central transition and also, owing to the large magnitude of the first-order quadrupolar interaction, they may display increased sensitivity to dynamics [1,3,12]. In many cases, their study may be greatly facilitated by the use of a rotor-synchronized experiment where an undistorted lineshape with moderate sensitivity is obtained.

Rotor-synchronization in the directly acquired, or t_2, time domain is more difficult to achieve than in an indirectly acquired time domain, such as the t_1 dimension of a two-dimensional experiment. Here, we describe the practical aspects of direct rotor-synchronized acquisition, discussing problems such as the need for very precise timings in the experiment and the effects of the audiofrequency filters. Additionally, for half-integer spin quadrupolar nuclei, we describe a new experiment which makes use of a double-quantum filter [13] to acquire a rotor-synchronized spectrum that contains signal from the ST_1 satellite transitions only. Although much information is contained in rotor-synchronized MAS

spectra containing all transitions, the overlap of resonances (particularly that of the ST_1 and CT lineshapes) or the high MAS rate required to obtain all transitions simultaneously may restrict their applicability. The acquisition of a spectrum containing only ST_1 satellite transitions is then able to simplify the problem of extracting useful information.

2. Practical aspects of direct rotor-synchronization

The use of rotor-synchronization in an indirectly observed time domain, for example, in the t_1 dimension of a two-dimensional experiment, is reasonably straightforward and is employed in many different types of experiments. For example, indirect rotor-synchronization of satellite-transition spinning sidebands is crucial to the success of the two-dimensional satellite-transition MAS (STMAS) experiment [14] used to obtain high-resolution NMR spectra of quadrupolar nuclei with half-integer spin. It has also been employed to improve both the sensitivity and lineshapes in multiple-quantum MAS (MQMAS) spectra [15,16] and in ^2H MAS spectroscopy [17–19]. Such synchronization is achieved by setting the duration of the t_1 increment equal to the rotor period ($\tau_R = 1/\nu_R$), thereby aliasing all sidebands onto a centreband and resulting in a spectral width in F_1 which is equal to the spinning rate ν_R. Care should be taken to ensure that the finite durations of the pulses that bracket the t_1 period are taken into account by altering the initial t_1 duration to ensure that the first point (in t_1) is acquired at the top of a rotary echo [5]. This is of great importance for experiments involving quadrupolar nuclei, particularly for transitions broadened by the first-order quadrupolar interaction, where the rotary echoes are very sharp [5].

Rotor-synchronization in the directly observed time domain is significantly more difficult to implement. Many important practical aspects, however, remain the same. For example, accurate rotor-synchronization always requires a stable MAS rate, as any fluctuations result in a broadening of the signal [5,16]. With modern equipment, spinning rate control to within ±2 Hz is routine and equipment with even greater precision (±0.2 Hz) has been demonstrated [20]. In addition, the spinning angle must be set precisely to the magic angle to remove the dipolar, CSA, and quadrupolar (first-order and $l = 2$ second-order) broadening completely. This is of particular importance, once again, for the large quadrupolar interaction, where a small misset in the spinning angle may result in the introduction of a significant broadening or splitting into the spectrum [5,14]. The magic angle can be set with reasonable ease (using ^{79}Br NMR of KBr or ^{23}Na NMR of NaNO₃, for example) to an accuracy of a few hundredths of a degree, although it should be noted that a substantially higher accuracy (to within ±0.003°) is required for the high-resolution STMAS experiment [5,14]. For the experiments described here, where the lineshapes observed are also affected by significant second-order quadrupolar broadening, the accuracy achieved using conventional angle-setting methods, such as ^{79}Br NMR of KBr, may be sufficient. Finally, it should be noted that the acquisition of data in concert with the rotor period restricts the observable spectral width to $1/\tau_R$, or the spinning frequency, ν_R. If lineshapes are particularly broad or if distinct lineshapes are well separated, problems may be encountered at low spinning rates, with the centreband spectrum itself folding or aliasing. The rotor-synchronized spectrum may also be difficult to phase as a result of the relatively long interval ($\sim\tau_R$) between the end of the pulse and the first data point. The use of fast MAS rates, therefore, is a distinct advantage.

The difficulties with direct rotor-synchronization, or perhaps more specifically the differences to that performed in an indirect manner, originate with the presence of audiofrequency filters in the receiver section of the spectrometer. The radiofrequency signal from the probe is converted to the audiofrequency range and then digitized by the analogue-to-digital converter (ADC), with the sampling rate determined by the desired spectral width [21]. The highest frequency which can be characterized by a particular sampling rate is known as the Nyquist frequency [8]. As described previously, frequencies outside this range are still detected but appear at false positions, i.e., they are aliased. Whilst this is a prerequisite for the rotor-synchronized experiments described here, it would be a major disadvantage if all possible frequencies were aliased in this manner. In addition to the true NMR signals, we would also digitize a virtually infinite amount of white noise, containing an essentially unlimited range of frequencies. To avoid this it is necessary to limit the electrical bandwidth of the spectrometer by using a (variable) analogue bandpass filter after conversion but before digitization [21]. The adjustment of the bandwidth of such a filter is often performed automatically by the spectrometer software upon selection of the desired spectral width. In addition to analogue filters, it should be noted that many modern spectrometers now also possess digital audiofrequency filters, which operate on digitized data after both conversion and sampling. Digital filtration is a very efficient way of removing the unwanted aliased noise from the spectrum, with the edges of the filter very sharply defined (unlike many analogue filters). However, currently many digital filtration systems place limitations upon the highest sampling rates that may be employed and hence upon the maximum spectral frequencies detected. For rotor-synchronized experiments involving quadrupolar satellite transitions the frequency ranges required are often very large, usually necessitating the use of only the analogue filters.

The presence of audiofrequency filters has a significant effect upon the NMR signal, shifting the apparent time origin of the free induction decay (FID). Fig. 3A shows, schematically, the pulse sequence, FID and data sampling for a direct rotor-synchronized experiment. After an initial pulse of duration p1, a series of rotary echoes are observed separated by the rotor period τ_R. The dwell time (or sampling period), τ_{dwell}, is set equal to τ_R, with a data point taken at the peak of every rotary echo. To ensure that the first data point (and, therefore, all following data points) are acquired at the exact point at which the echo occurs, the free-precession duration τ_{opt} must be optimized experimentally. By analogy with rotor-synchronization in the indirect dimension [5], we would take account of the finite pulse length by selecting $\tau_{opt} = \tau_R - \frac{p1}{2}$. However, although successful in indirect rotor-synchronization, this may result in little or no signal when direct rotor-synchronization is performed. Fig. 4A shows a series of rotor-synchronized ^{87}Rb ($I = 3/2$, $v_0 = 130.9$ MHz) MAS NMR spectra of RbNO$_3$ as a function of the time τ_{opt}. The spinning rate is 20 kHz, resulting in a rotor period, τ_R, of 50 μs. A pulse duration, p1, of 1.5 μs has been employed. With $\tau_{opt} = \tau_R - \frac{p1}{2} = 49.25$ μs , only the central-transition signal (a signal with no significant spinning sidebands) is

observed. Only when τ_{opt} is increased does the satellite-transition signal appear, with the maximum signal obtained when $\tau_{opt} \approx 50.75$ μs, where the intensity of the satellite-transition peak is greater than that of the central transition. At this point, acquisition is truly synchronized with the rotor, with data sampling occurring at the top of every rotary echo, enabling all sidebands to be folded accurately onto the ST centreband. This can be seen in Figs. 4B and C, where a conventional ^{87}Rb MAS spectrum (acquired using a digital filter) and a rotor-synchronized ^{87}Rb MAS NMR spectrum ($\tau_{opt} = 50.75$ μs) of RbNO$_3$ are compared. In the first case, only the central-transition lineshape (resulting from the overlap of signal from the three crystallographically distinct Rb species [22]) appears with significant intensity, although the centreband of the satellite-transition spinning sidebands is just visible. When the acquisition is accurately rotor-synchronized both central and satellite transitions appear with good intensity.

It is apparent from Fig. 4 that the audiofrequency filter has shifted the apparent time origin of the FID, requiring τ_{opt} to be longer than predicted to truly rotor-synchronize the acquisition. This shift arises from the removal of high frequency components in the FID and is found on all NMR spectrometers. The shift
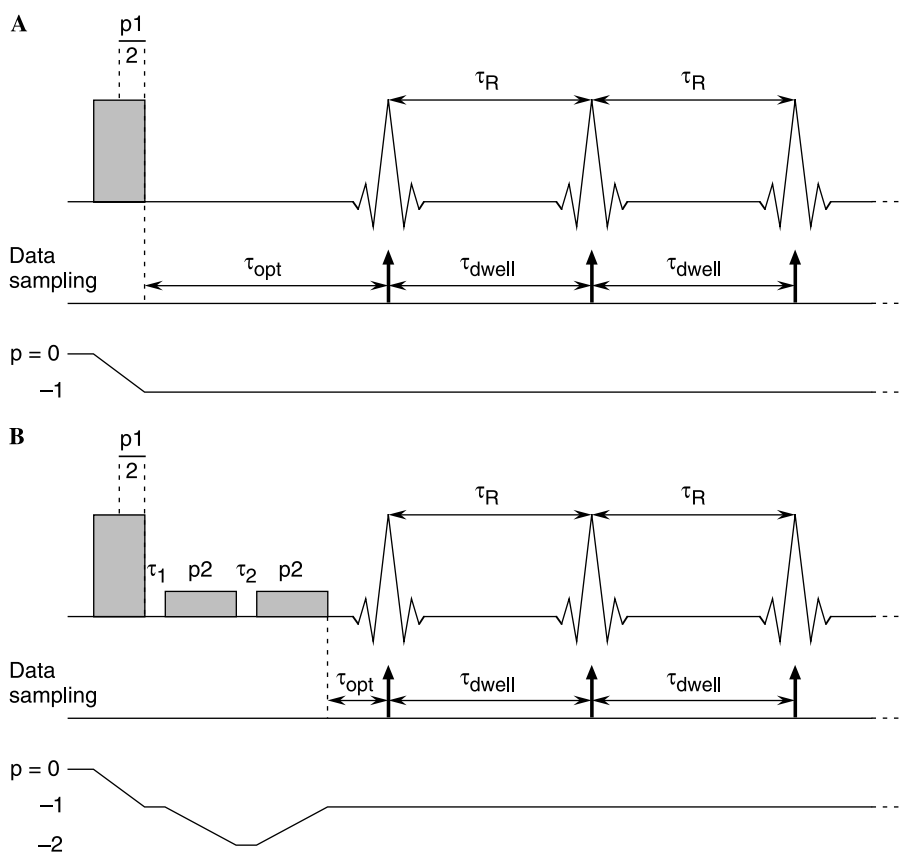

Fig. 3. Pulse sequences and coherence-transfer pathway diagrams for (A) a conventional MAS and (B) a double-quantum filtered MAS NMR experiment, both with rotor-synchronized acquisition in the direct time domain. Data sampling coincident with the rotary echoes is shown schematically. A phase cycle for the sequence in (B) is suggested in Table 1.
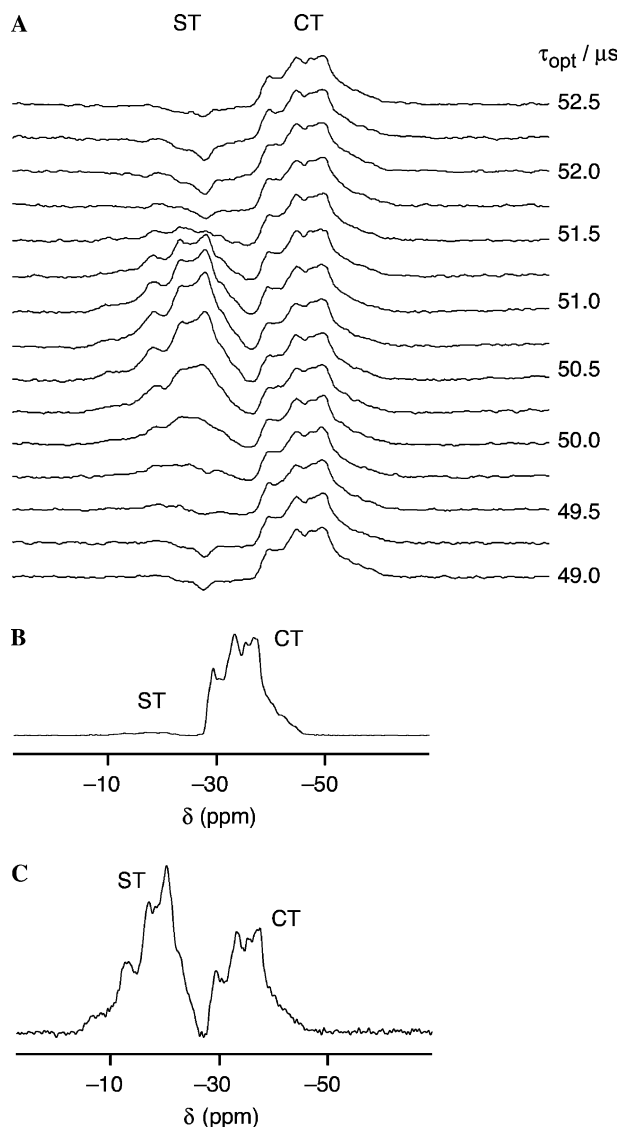
Fig. 4. ^{87}Rb ($I = 3/2$, $v_0 = 130.9$ MHz) MAS NMR of RbNO$_3$. (A) A series of rotor-synchronized MAS spectra recorded using the pulse sequence in Fig. 3A, as a function of the interval τ_{opt}. (B) A conventional MAS spectrum recorded without rotor-synchronized acquisition. (C) A rotor-synchronized MAS spectrum recorded using the pulse sequence in Fig. 3A with $\tau_{opt} = 50.75$ μs. In each case, the MAS rate was 20 kHz, p1 = 1.5 μs (optimized for CT excitation), and 960 transients were averaged with a recycle interval of 0.25 s. In (A and C), the bandwidth of the analogue filters was 1.25 MHz. In (B), digital filtration was employed. The ppm scale is referenced to 1 M RbNO$_3$ (aq).

observed is expected to be approximately equal to the inverse of the filter bandwidth. This results in an optimized time $\tau_{opt} = \tau_R - \frac{p1}{2} + \tau_x$, where, for a filter width of 1 MHz, τ_x is of the order of 1 μs. Although τ_x is very short, for rotor-synchronization of the first-order quadrupolar broadened satellite-transitions its inclusion is crucial to the success of the experiment.

The choice of filter bandwidth is also of importance for the sensitivity of a directly acquired rotor-synchronized experiment and is often a compromise between
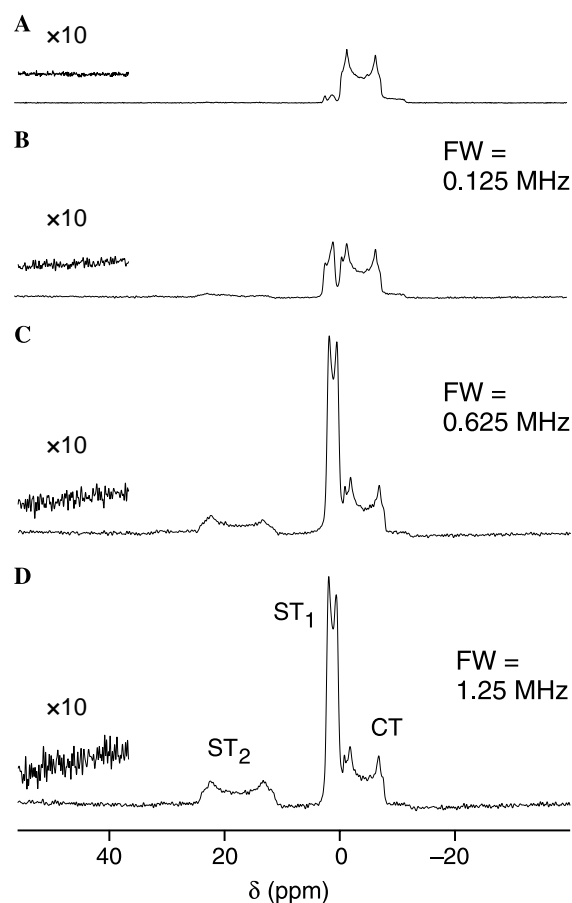

Fig. 5. ^{27}Al ($I = 5/2$, $v_0 = 104.3$ MHz) MAS NMR spectra of Al(acac)$_3$. (A) A conventional MAS spectrum recorded without rotor-synchronized acquisition. (B–D) Rotor-synchronized MAS spectra recorded using the pulse sequence in Fig. 3A. In each case, the MAS rate was 20 kHz, p1 = 1.0 μs (optimized for CT excitation), and 1200 transients were averaged with a recycle interval of 1.0 s. The spectrum in (A) was acquired with digital filtration whilst analogue filters with bandwidths, FW, of 0.125, 0.625, and 1.25 MHz were employed in (B–D), respectively. The interval τ_{opt} was (B) 57.5, (C) 51.5, and (D) 50.75 μs. The noise level is shown inset. The ppm scale is referenced to 1 M Al(NO$_3$)$_3$ (aq).

the amount of signal and the amount of noise folded into the spectrum. Fig. 5A shows a ^{27}Al ($I = 5/2$, $v_0 = 104.3$ MHz) MAS NMR spectrum of aluminium acetylacetonate. This material possesses only a single distinct Al species with $C_Q = e^2qQ/h = 3.0$ MHz and $\eta = 0.15$ [23]. The spectrum in Fig. 5A has been acquired with digital filtration (with, therefore, no aliasing of either NMR signal or noise) and contains a second-order broadened lineshape resulting from the central transition. In addition, the centreband of the ST$_1$ satellite transitions is also observed but with a much reduced intensity. The centreband of the broader, and hence even less intense, ST$_2$ satellite transitions is not observed. The rotor-synchronized ^{27}Al MAS spectra in Figs. 5B–D have been acquired with analogue filters with bandwidths of 125 kHz, 625 kHz, and 1.25 MHz, respectively. (Note that, owing to the differing filter

bandwidths, $\tau_{opt} = 57.5$, 51.5, and 50.75 μs in Figs. 5B–D, respectively). It is apparent that as the filter bandwidth increases the intensity of both ST_1 and ST_2 satellites increases as more sidebands are aliased. However, the aliasing of increasingly large amounts of noise is also apparent (shown inset), with the signal-to-noise ratio of the central-transition lineshape decreasing as the filter bandwidth is increased.

Fig. 5 also demonstrates the important effect of the choice of filter bandwidth upon the lineshape observed. When the bandwidth is small, severe distortions are present in the satellite-transition lineshapes. There are two likely causes for this. As described previously, when second-order quadrupolar interactions are present, the lineshape of each individual spinning sideband in a normal MAS spectrum is not necessarily representative of the true lineshape [3,6]. When the filter bandwidth is small only a few of these sidebands are aliased and the rotor-synchronised lineshape is distorted. Aliasing of a large number of sidebands, as in Fig. 5D, is required for the true satellite-transition lineshape to be obtained. Second, when small analogue filter bandwidths are employed, signals close to the edge of the bandwidth tend to have distorted phase and will, therefore, contribute to lineshape distortions in the aliased spectrum [21]. A reasonably wide filter bandwidth, folding in as many undistorted signals as possible but minimizing the amount of added noise, is therefore ideal. Care should be taken when adjusting the filter bandwidth, as many spectrometers will alter this value automatically when spectral parameters are modified. A final manual setting should be undertaken before the experiment is performed.

3. Double-quantum filtration

In the rotor-synchronized ^{27}Al MAS NMR spectrum in Fig. 5D all three transitions (CT, ST_1, and ST_2) appear with both good intensity and undistorted lineshapes. As described previously, the appearance of all three powder-pattern lineshapes is different, with differing isotropic shifts and anisotropic second-order quadrupolar broadening [5,7]. It has already been noted that in a few cases one or more transitions may show a distinct increase in resolution over the conventional central-transition MAS NMR spectrum. Although a wealth of information is available in this type of spectrum, it may sometimes be difficult to extract accurately owing to the overlap of different types of transitions (such as the CT and ST_1 lineshapes), particularly when more than one crystallographically distinct species is present.

Recently, a double-quantum filter has been employed in the rotor-synchronized t_1 dimension of the STMAS experiment to simplify the spectrum and ensure that

signal from only the ST_1 satellites is present [13]. Double-quantum filtration is achieved by using a pulse with a low radiofrequency field strength ($v_1 = |\gamma B_1|/2\pi \ll v_Q^{PAS}$) to selectively invert only the central transition. This pulse is applied at the end of the t_1 evolution period, during which both central- and satellite-transition coherences evolve. Phase cycling is then employed to select double-quantum coherences [24]. Only from ST_1 satellite-transition magnetization can double-quantum ($m_I = \mp 1/2 \leftrightarrow \pm 3/2$) coherences be created in this manner, resulting in the removal of the CT signal (and ST_2, ST_3, etc., signals, if present) from the spectrum. This method excites double-quantum coherences very efficiently as long as v_Q^{PAS} is not close to zero, with efficiencies usually between 80 and 100% observed experimentally [13], thereby ensuring the excellent sensitivity of the STMAS experiment is retained [5,14]. It is possible to employ a similar approach in the one-dimensional rotor-synchronized experiments described earlier to simplify the spectrum.

Fig. 3B shows a pulse sequence for a double-quantum filtered directly rotor-synchronized experiment that is designed to yield signal from only the ST_1 satellite transitions, removing that from the central transition and any higher-order satellite transitions. After an initial pulse, p1, which creates both central- and satellite-transition magnetization, a central-transition-selective inversion pulse (p2) is applied. Phase cycling is used to select double-quantum coherences ensuring, as in DQF-STMAS [13], that only signals arising from ST_1 transitions are present. However, these double-quantum coherences cannot be directly detected and so reconversion to observable single-quantum coherences is required. This reconversion must be performed using another central-transition-selective inversion pulse to prevent the creation of central-transition (or higher-order satellite-transition) coherences. The ST_1 satellite-transition signal must then be acquired synchronously with the rotor, aliasing all of the spinning sidebands onto the centreband. This should result in a spectrum such as that shown in Fig. 2C, where only signal from the ST_1 transition appears whilst that from the other transitions has been removed. Although two selective inversion pulses are applied, the high efficiency [13] of the double-quantum excitation and reconversion should ensure that the sensitivity of the overall experiment remains acceptable. However, in practice, when the quadrupolar interaction is very small, this efficiency may decrease as it becomes more difficult for the inversion pulse to be truly selective for the central transition.

IThe double-quantum coherences ($m_I = \mp 1/2 \leftrightarrow \pm 3/2$) are subject to the same first-order quadrupolar interaction as the ST_1 satellite transitions. Therefore, insertion of an inversion pulse does not significantly affect the first-order quadrupolar evolution. As in the simpler conventional rotor-synchronized experiment

Table 1
A possible (32-step) phase cycle for the double-quantum filtered rotor-synchronized experiment ($p = 0 \rightarrow -1 \rightarrow -2 \rightarrow -1$) in Fig. 3B

ϕ_1: 0° 45° 90° 135° 180° 225° 270° 315° 90° 135° 180° 225° 270° 315° 0° 45°
180° 225° 270° 315° 0° 45° 90° 135° 270° 315° 0° 45° 90° 135° 180° 225°

ϕ_2: 0° 45° 90° 135° 180° 225° 270° 315° 90° 135° 180° 225° 270° 315° 0° 45°
180° 225° 270° 315° 0° 45° 90° 135° 270° 315° 0° 45° 90° 135° 180° 225°

ϕ_3: 0° 0° 0° 0° 0° 0° 0° 0°
90° 90° 90° 90° 90° 90° 90° 90°
180° 180° 180° 180° 180° 180° 180° 180°
270° 270° 270° 270° 270° 270° 270° 270°

ϕ_R: 0° 90° 180° 270° 0° 90° 180° 270° 90° 180° 270° 0° 90° 180° 270° 0°
180° 270° 0° 90° 180° 270° 0° 90° 270° 0° 90° 180° 270° 0° 90° 180°

The phases of the first, second, and third pulses are denoted ϕ_1, ϕ_2, and ϕ_3, respectively, whilst that of the receiver is denoted ϕ_R.

described above, great care must also be taken in the double-quantum filtered experiment to ensure that the acquisition is synchronized accurately with the rotor. To minimize any problems with phasing the final spectrum, all three pulses are performed before acquisition of the data point at the top of the first accessible rotary echo. In the ideal case, $\tau_{opt} = \tau_R - \frac{p1}{2} - \tau_1 - \tau_2 - (2 \times p2)$, where τ_1 and τ_2 are the relatively short intervals (a few μs) that separate the pulses. However, τ_{opt} must once again be experimentally optimized to take into account the apparent time shifting of the origin of the FID by the analogue filter, resulting in $\tau_{opt} = \tau_R - \frac{p1}{2} - \tau_1 - \tau_2 - (2 \times p2) + \tau_x$. The MAS rate should be carefully chosen, first to ensure that the two long selective pulses may both be applied within the first rotor period and, secondly, to ensure that the spectral width is large enough to contain all the resonances. Although this may seem restrictive, it should be noted that the presence of only ST_1 transitions will enable a smaller spectral width (and hence longer rotor period) to be utilized, especially for spin $I = 5/2$. A central-transition-selective pulse is only able to excite double-quantum coherences with the same sign of coherence order as the original ST_1 transitions (i.e., $p = +1$ to $p = +2$ or $p = -1$ to $p = -2$). Therefore, the phase cycling was designed [24] to select only the single coherence-transfer pathway shown in Fig. 3B. The 32-step cycle given in Table 1 (eight steps for double-quantum selection; four steps for CYCLOPS; $8 \times 4 = 32$) was utilized, although shorter phase cycles (both 16- and 8-step) are also possible. However, in some cases the use of these shorter cycles may lead to small intensity losses and lineshape distortions.

4. Results

Experiments were performed on a Bruker Avance spectrometer equipped with a widebore 9.4 T magnet and a 2.5 mm MAS probe. The excitation pulses ($v_1 \approx 60$–120 kHz) had durations optimised for either excitation of CT or ST_1 transitions, with the latter dura-

tions found to be roughly twice those of the former. (Note that in Figs. 4 and 5 the pulse durations were optimised for excitation of CT transitions, thereby yielding ST transitions with less than the full intensity.) The central-transition-selective pulses ($v_1 \approx 10$–20 kHz) had durations calibrated by searching for the first null in the central-transition nutation.

Fig. 6A shows the conventional ^{87}Rb MAS NMR spectrum of RbNO$_3$, recorded with digital filtration. A central-transition resonance is observed together with, at much lower intensity, the centreband of the satellite transitions. The use of a digital filter has restricted the amount of aliased noise to a minimum. A spectrum obtained with rotor-synchronized acquisition (as shown in Fig. 3A) is displayed in Fig. 6B. The use of an analogue filter with a wide bandwidth (1.25 MHz) enables the aliasing of many satellite-transition spinning sidebands, resulting in a satellite-transition resonance with a much increased intensity and an undistorted lineshape. However, the wide filter bandwidth has also resulted in the folding of more thermal noise and a significant decrease in the signal-to-noise ratio of the central-transition lineshape. Fig. 6C shows a spectrum acquired with the double-quantum filtered pulse sequence in Fig. 3B, containing only the satellite-transition lineshape. This lineshape contains ~80% of the intensity of that in Fig. 6B, confirming the efficiency of the double-quantum excitation and reconversion pulses [13]. Moreover, no significant lineshape distortion is apparent, with the experimental lineshape in excellent agreement with that simulated using literature parameters for the three crystallographically distinct Rb species (Fig. 6C inset) [22].

As ^{87}Rb is a spin $I = 3/2$ nucleus, there is little difference in the magnitude of the anisotropic broadening between the central and satellite transitions, with $A^4(3/2, 3/2) = -(8/9) A^4(3/2, 1/2)$ [5,7]. However, a much larger increase in resolution is obtained for spin $I = 5/2$, where the ST_1 transitions possess only 7/24 of the anisotropic broadening of the central transition. This is demonstrated in Figs. 6D–F, a series of ^{27}Al MAS NMR spectra of aluminium acetylacetonate (Al(acac)$_3$), with the conventional MAS spectrum shown in Fig. 6D. Three lineshapes with good intensity are obtained when rotor-synchronized acquisition is employed (Fig. 6E), but only that resulting from the ST_1 transitions is observed in Fig. 6F, where the spectrum has been acquired using the double-quantum filtered pulse sequence in Fig. 3B. However, the use of a central-transition-selective inversion pulse to excite and reconvert double-quantum coherences is slightly less effective here, owing primarily to the small quadrupolar interaction, resulting in a sensitivity loss and a small lineshape distortion. Note, however, that no signal from either the central-transition or ST_2 lineshapes is observed. The considerable decrease in the anisotropic quadrupolar broadening (and hence potential increase in resolution) in the ST_1 spectrum is clear.
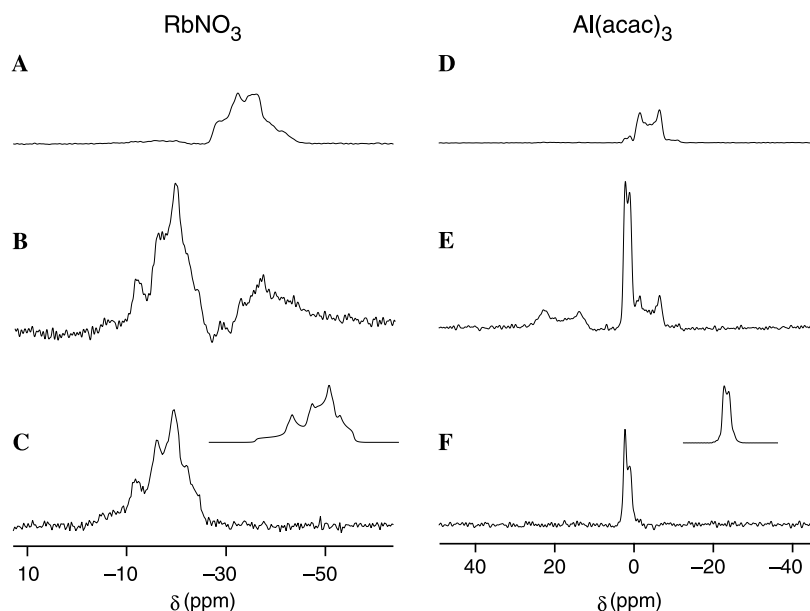
Fig. 6. (A–C) ^{87}Rb ($\nu_0 = 130.9$ MHz) MAS NMR of RbNO$_3$ and (B–D) ^{27}Al ($\nu_0 = 104.3$ MHz) MAS NMR of Al(acac)$_3$. Spectra in (A and D) are conventional MAS spectra acquired with digital filtration; spectra in (B and E) were acquired rotor-synchronized using the pulse sequence in Fig. 3A; spectra in (C and F) were acquired rotor-synchronized using the double-quantum filtered pulse sequence in Fig. 3B. Analogue filter bandwidths in (B,C,E, and F) were 1.25 MHz. In (A–C), 320 transients were averaged with a recycle interval of 0.25 s; pulse durations were p1 = 2.1 μs (optimized for ST excitation) and p2 = 16 μs. In (D–F), 320 transients were averaged with a recycle interval of 1 s; pulse durations were p1 = 1.6 μs (optimized for ST$_1$ excitation) and p2 = 17 μs. In each case, the MAS rate was 20 kHz. In (C and F), the insets show the ST$_1$ lineshape simulated using literature NMR parameters [22,23]. The ppm scales are referenced to 1 M RbNO$_3$ (aq) or 1 M Al(NO$_3$)$_3$ (aq).

Many important quadrupolar nuclei have a spin quantum number $I = 5/2$ (e.g., ^{17}O, ^{25}Mg, ^{27}Al, ^{47}Ti, ^{55}Mn, ^{67}Zn, and ^{95}Mo) and so will possess ST$_1$ spectra that exhibit substantially increased resolution. Fig. 7 shows conventional central-transition MAS and double-quantum filtered rotor-synchronized ^{17}O ($\nu_0 = 54.2$ MHz) NMR spectra of 35% ^{17}O-enriched forsterite, α-Mg$_2$SiO$_4$ (Figs. 7A and B) and ^{27}Al ($\nu_0 = 104.3$ MHz) NMR spectra of sillimanite, Al$_2$SiO$_5$ (Figs. 7C and D) and γ-alumina, γ-Al$_2$O$_3$ (Figs. 7E and F). Use of the double-quantum filtered pulse sequence in Fig. 3B yields an ^{17}O ST$_1$ spectrum of forsterite (Fig. 7B) where one crystallographically distinct O species is now completely resolved. Good agreement is obtained with the spectrum (Fig. 7B, inset) simulated using literature parameters [25]. However, the small quadrupolar couplings for ^{17}O in forsterite result in poor sensitivity in the ST$_1$ spectrum. Increased resolution is also observed in the ^{27}Al ST$_1$ spectrum of sillimanite (Fig. 7D), where the two crystallographically distinct Al species are now completely resolved. Computer simulations of the lineshapes in Figs. 7C and D with the literature NMR parameters [26] indicate the presence in our natural sample of sillimanite of a significant linebroadening additional to that arising from the second-order quadrupolar interaction and we have included an estimate of this in our simulation of the ST$_1$ spectrum (Fig. 7D, inset).

Finally, it is well known that the structural disorder in γ-alumina is evidenced in conventional ^{27}Al MAS NMR in the form of two broad, relatively featureless peaks cor-

responding to tetrahedral (centred at ∼60 ppm) and octahedral (centred at ∼10 ppm) Al coordinations (Fig. 7E). The broadening of each peak is a consequence of distributions of isotropic chemical shifts and quadrupolar interactions that themselves arise from the range of Al environments in the solid [27]. As with the previous examples, the double-quantum filtered pulse sequence in Fig. 3B yields an ^{27}Al spectrum (Fig. 7F) with higher resolution (i.e., in this case, reduced overlap between the peaks corresponding to tetrahedral and octahedral Al coordinations). The peaks in the ST$_1$ spectrum are broadened by the same distributions of chemical shifts and quadrupolar interactions as those in the conventional CT spectrum but are narrower because the anisotropic quadrupolar broadening of the ST$_1$ transitions is only 7/24 of that of the CT transitions. Quantitative comparison, therefore, of lineshapes in ^{27}Al CT and ST$_1$ spectra could be used to measure the distributions of chemical shifts and quadrupolar interactions. For γ-alumina, these distributions have already been estimated using ^{27}Al MQMAS NMR [27,28] and the values have been used to simulate the ST$_1$ lineshape corresponding to octahedral Al coordination (Fig. 7F, inset).

5. Discussion

Per unit acquisition time, the signal-to-noise ratios in the double-quantum filtered rotor-synchronized spectra
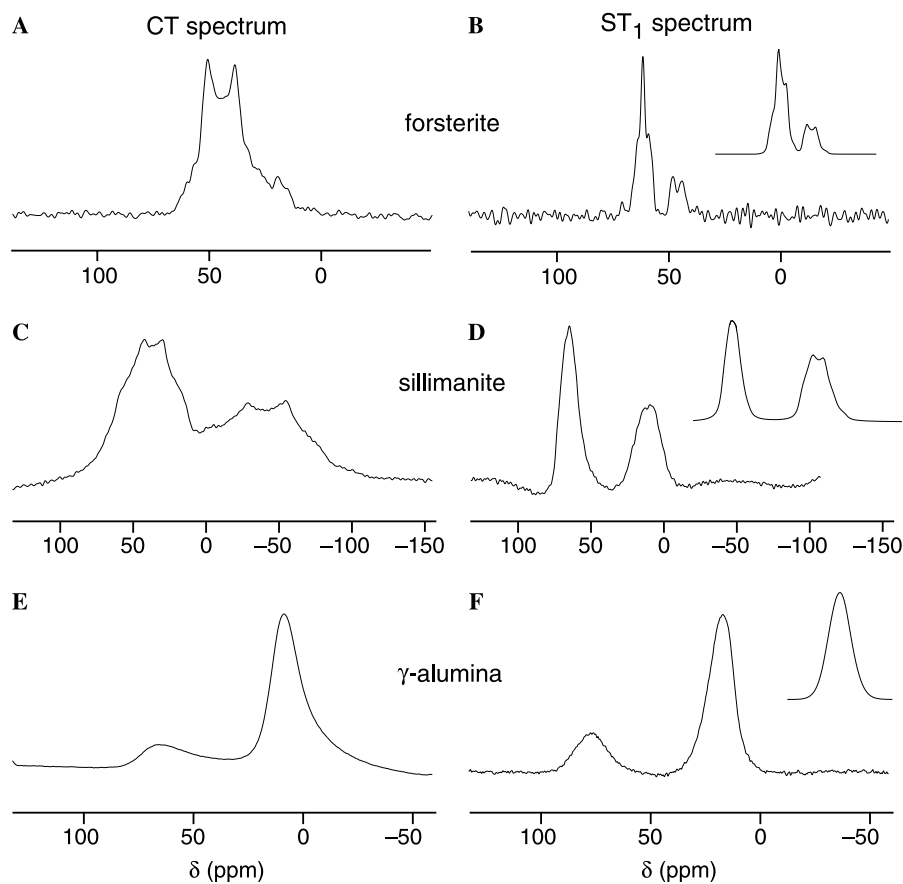
Fig. 7. (A and B) ^{17}O ($I = 5/2$, $v_0 = 54.2$ MHz) MAS NMR of forsterite, α-Mg$_2$SiO$_4$; (C and D) ^{27}Al ($v_0 = 104.3$ MHz) MAS NMR of sillimanite, Al$_2$SiO$_5$; and (E and F) ^{27}Al ($v_0 = 104.3$ MHz) MAS NMR of γ-alumina, γ-Al$_2$O$_3$. Spectra in (A,C, and E) are conventional MAS spectra with digital filtration, whilst those in (B,D, and F) have been acquired rotor-synchronized using the double-quantum filtered pulse sequence in Fig. 3B with an analogue filter bandwidth of 1.25 MHz. In (A) 320, (B) 2400, (C) 240, (D) 3200, (E) 320, and (F) 3200 transients have been recorded with recycle intervals of (A and B) 2.0, (C and D) 0.5, and (E and F) 2.0 s, respectively. The MAS rate was (A and B) 20, (C and D) 30, and (E and F) 20 kHz. Pulse durations of (A) p1 = 1.6 µs (optimized for CT excitation), (B) p1 = 3.2 µs (optimized for ST$_1$ excitation), and p2 = 16 µs, (C) p1 = 1.1 µs (optimized for CT excitation), (D) p1 = 2.0 µs (optimized for ST$_1$ excitation) and p2 = 8.5 µs, (E) p1 = 0.8 µs (optimized for CT excitation), and (F) p1 = 0.8 µs and p2 = 11 µs were employed. In (B,D, and F), the insets show the ST$_1$ lineshape simulated using literature NMR parameters [23–28]. The ppm scales are referenced to H$_2$O or 1 M Al(NO$_3$)$_3$ (aq).

in Figs. 6 and 7 are worse than in the central-transition spectra. A rough estimate is instructive. If we assume a filter width of 1 MHz and a spectral width (and hence MAS rate) of 20 kHz in a rotor-synchronized spectrum then it will contain $\sqrt{(10^6/(20 \times 10^3))} = \sqrt{50} \approx 7$ times more noise than a perfectly filtered central-transition spectrum. But, if we then assume fully nonselective excitation, the relative (integrated) intensities of the CT, ST$_1$, and ST$_2$ transitions in a spin $I = 5/2$ nucleus are 9:16:10, respectively. Furthermore, for spin $I = 5/2$, the ST$_1$ transition is only 7/24 as broad as the CT transition if second-order quadrupolar broadening dominates and so will have a peak height 24/7 times greater per unit area. Therefore, in the ideal case, we would expect the peak height in the spin $I = 5/2$ ST$_1$ spectrum to be $(16/9) \times (24/7) = 128/21 \approx 6$ times greater than that in the CT spectrum, yielding a signal-to-noise ratio in the ST$_1$ spectrum that was $\sim$6/7 or $\sim$85% of that in the CT spectrum. It must be stressed, however, that this is

very much an ideal case estimate: less than 100% efficiency of the double-quantum filter, sources of line broadening other than the quadrupolar interaction, inefficient excitation of the satellite transitions, and, of course, observation of nuclei with spin quantum numbers other than $I = 5/2$ will all greatly reduce the peak height in the ST$_1$ spectrum relative to the CT spectrum.

Having discussed one-dimensional CT and ST$_1$ spectra and their relative merits, it is worth saying something at this point about their relationship with the two-dimensional methods STMAS [14] and I-STMAS [29], as the former involves direct acquisition of the CT spectrum and the latter direct acquisition of the ST spectrum. The first point to note is that STMAS and I-STMAS spectra are not complementary; they each have a CT dimension and an ST dimension and, thus, contain identical information. As two-dimensional methods, they contain far more information (including the fully isotropic spectrum) than the one-dimensional experi-

ments described in this work. However, two-dimensional spectra generally take much longer to record than one-dimensional spectra (for purely practical reasons) while both STMAS and I-STMAS involve a highly inefficient $CT \leftrightarrow ST$ coherence transfer step that greatly reduces their sensitivity compared with the methods described here. Therefore, our one-dimensional rotor-synchronized experiments should not be viewed as rivals of either STMAS or I-STMAS but as another, quite distinct, category of experiment altogether. Finally, it has been noted that the I-STMAS experiment is inferior to the STMAS experiment because, by directly acquiring the ST spectrum with a very wide filter bandwidth, it yields spectra that contain a lot more noise [29]. This negative assessment cannot be applied to one-dimensional rotor-synchronized experiments because (i) as we have seen, unlike STMAS and I-STMAS spectra, which both yield essentially identical peak heights, it is possible for ST_1 spectra to yield peak heights several times greater than those in CT spectra, and (ii) unlike STMAS and I-STMAS spectra, one-dimensional CT and ST_1 spectra contain complementary information, hence it may be worth paying a signal-to-noise penalty for acquiring the latter.

6. Conclusions

The use of rotor-synchronized MAS to remove anisotropic broadening in the directly acquired time-domain is more difficult to implement practically than in an indirect dimension of a multidimensional experiment. Accurate rotor-synchronization is only achieved when the effects of the audiofrequency filters have been taken into account. This is particularly important for the satellite transitions of quadrupolar nuclei, which can often be broadened by the first-order quadrupolar interaction over many MHz. Rotor-synchronization has advantages over the observation of individual spinning sideband lineshapes, as it results in an increase in signal-to-noise and allows the true or undistorted lineshape to be recorded.

For quadrupolar nuclei with half-integer spin, the rotor-synchronized satellite-transition lineshapes are similar in appearance to those observed for the central transition but with different isotropic and anisotropic second-order quadrupolar interactions. It is well known that in some cases, particularly where spin $I = 5/2$ nuclei are involved, this may result in a significant increase in resolution. However, a rotor-synchronized spectrum containing all central-transition and satellite-transition lineshapes may be difficult to interpret owing to the overlap of different transitions. We have demonstrated a novel double-quantum filtered experiment that simplifies a rotor-synchronized MAS spectrum, leaving only the ST_1 ($m_I = \pm 1/2 \leftrightarrow \pm 3/2$) satellite-transition line-

shapes. This experiment (which could be dubbed DQF-SATRAS) will be of particular use for the resolution of crystallographically distinct species in spin $I = 5/2$ MAS NMR spectra and for the study of disordered or amorphous materials.

References

[1] J. Virlet, Line narrowing methods in solids, in: D.M. Grant, R.K. Harris (Eds.), Encyclopedia of Nuclear Magnetic Resonance, Wiley, Chichester, 1996, pp. 2694–2711.

[2] E.R. Andrew, Magic angle spinning, in: D.M. Grant, R.K. Harris (Eds.), Encyclopedia of Nuclear Magnetic Resonance, Wiley, Chichester, 1996, pp. 2891–2901.

[3] M.M. Maricq, J.S. Waugh, NMR in rotating solids, J. Chem. Phys. 70 (1979) 3300–3316.

[4] A.J. Vega, Quadrupolar nuclei in solids, in: D.M. Grant, R.K. Harris (Eds.), Encyclopedia of Nuclear Magnetic Resonance, Wiley, Chichester, 1996, pp. 3869–3889.

[5] S.E. Ashbrook, S. Wimperis, High-resolution NMR of quadrupolar nuclei in solids: the satellite-transition magic angle spinning (STMAS) experiment, Prog. NMR Spectrosc. 45 (2004) 53–108.

[6] J. Skibsted, N.C. Nielsen, H. Bildsøe, H.J. Jakobsen, Satellite transitions in MAS NMR spectra of quadrupolar nuclei, J. Magn. Reson. 95 (1991) 88–117.

[7] A. Samoson, Satellite-transition high-resolution NMR of quadrupolar nuclei in powders, Chem. Phys. Lett. 119 (1985) 29–32.

[8] R. Freeman, A Handbook of Nuclear Magnetic Resonance, Longman, Harlow, 1997, p. 88.

[9] C. Jäger, How to get more from ^{27}Al MAS NMR by high-speed satellite-transition spectroscopy, J. Magn. Reson. 99 (1992) 353–362.

[10] C. Jäger, W. Müllerwarmuth, C. Mundus, L. van Wullen, ^{27}Al MAS NMR spectroscopy of glasses—new facilities by application of SATRAS, J. Non-Cryst. Solids 149 (1992) 209–217.

[11] S. Wi, S.E. Ashbrook, S. Wimperis, L. Frydman, Second-order quadrupole-shielding effects in magic-angle spinning solid-state nuclear magnetic resonance, J. Chem. Phys. 118 (2003) 3131–3140.

[12] S.E. Ashbrook, S. Antonijevic, A.J. Berry, S. Wimperis, Motional broadening: an important distinction between multiple-quantum and satellite-transition MAS NMR of quadrupolar nuclei, Chem. Phys. Lett. 364 (2002) 634–642.

[13] H.T. Kwak, Z. Gan, Double-quantum filtered STMAS, J. Magn. Reson. 164 (2003) 369–372.

[14] Z. Gan, Isotropic NMR spectra of half-integer quadrupolar nuclei using satellite transitions and magic-angle spinning, J. Am. Chem. Soc. 122 (2000) 3242–3243.

[15] L. Frydman, J.S. Harwood, Isotropic spectra of half-integer quadrupolar spins from bidimensional magic-angle-spinning NMR, J. Am. Chem. Soc. 117 (1995) 5367–5368.

[16] D. Massiot, Sensitivity and lineshape improvements of MQ-MAS by rotor-synchronized data acquisition, J. Magn. Reson. A 122 (1996) 240–244.

[17] B. Blümich, P. Blümler, J. Jansen, Presentation of sideband envelopes by two-dimensional one-pulse (TOP) spectroscopy, Solid State Nucl. Magn. Reson. 1 (1992) 111–113.

[18] M.J. Duer, C. Stourton, ^{2}H double-quantum NMR spectroscopy for the study of molecular motion in solids, J. Magn. Reson. 129 (1997) 44–52.

[19] J.H. Kristensen, H. Bildsøe, H.J. Jakobsen, N.C. Nielsen, Separation of ^{2}H MAS NMR spectra by two-dimensional spectroscopy, J. Magn. Reson. 139 (1999) 314–333.

[20] E. Hughes, T. Gullion, A simple, inexpensive and precise magic angle spinning speed controller, Solid State Nucl. Magn. Reson. 26 (2004) 16–21.

[21] A.E. Derome, Modern NMR Techniques for Chemistry Research, Pergammon Press, Oxford, 1987 (Chapter 2).

[22] D. Massiot, B. Touzo, J.P. Coutures, J. Virlet, P. Forian, P.J. Grandinetti, Two-dimensional magic-angle spinning isotropic reconstruction sequences for quadrupolar nuclei, Solid State Nucl. Magn. Reson. 6 (1996) 73–83.

[23] P.J. Barrie, Distorted powder lineshapes in CP MAS NMR-spectroscopy of solids, Chem. Phys. Lett. 208 (1993) 486–490.

[24] G. Bodenhausen, H. Kogler, R.R. Ernst, Selection of coherence-transfer pathways in NMR pulse experiments, J. Magn. Reson. 56 (1984) 370–388.

[25] S.E. Ashbrook, A.J. Berry, S. Wimperis, Three- and five-quantum ^{17}O MAS NMR of forsterite Mg_2SiO_4, Am. Mineral 84 (1999) 1191–1194.

[26] E. Lippmaa, A. Samoson, M. Mägi, High-resolution ^{27}Al NMR of aluminosilicates, J. Am. Chem. Soc. 108 (1986) 1730–1735.

[27] J. McManus, Residual broadening in high-resolution NMR of quadrupolar nuclei in solids (PhD thesis), University of Exeter, 2001.

[28] S. Wimperis, Quadrupolar NMR in inorganic materials: the multiple-quantum magic angle spinning (MQMAS) experiment, in: M. Utz (Ed.), Modern Magnetic Resonance: Materials Science, Kluwer, Amsterdam, 2005 (in press).

[29] J.P. Amoureux, C. Morais, J. Trebosc, J. Rocha, C. Fernandez, I-STMAS: a new high-resolution solid-state NMR method for half-integer quadrupolar nuclei, Solid State Nucl. Magn. Reson. 23 (2003) 213–223.